Journal of Power Sources 196 (2011) 8590–8597

Contents lists available at ScienceDirect

Journal of Power Sources

journal homepage: www.elsevier.com/locate/jpowsour

# Effect of electrolytes on the structure and evolution of the solid electrolyte interphase (SEI) in Li-ion batteries: A molecular dynamics study

Sang-Pil Kim[a], Adri C.T. van Duin[b], Vivek B. Shenoy[a,*]

[a] School of Engineering, Brown University, Providence, RI 02912, USA
[b] Department of Mechanical and Nuclear Engineering, Pennsylvania State University, University Park, PA 16802, USA

ARTICLE INFO

*Article history:*
Received 27 April 2011
Received in revised form 21 May 2011
Accepted 23 May 2011
Available online 30 May 2011

*Keywords:*
SEI
Li-ion battery
Li metal anode
Molecular dynamics

ABSTRACT

We have studied the formation and growth of solid-electrolyte interphase (SEI) for the case of ethylene carbonate (EC), dimethyl carbonate (DMC) and mixtures of these electrolytes using molecular dynamics simulations. We have considered SEI growth on both Li metal surfaces and using a simulation framework that allows us to vary the Li surface density on the anode surface. Using our simulations we have obtained the detailed structure and distribution of different constituents in the SEI as a function of the distance from the anode surfaces. We find that SEI films formed in the presence of EC are rich in $Li_2CO_3$ and $Li_2O$, while $LiOCH_3$ is the primary constituent of DMC films. We find that dilithium ethylene dicarbonate, LiEDC, is formed in the presence of EC at low Li surface densities, but it quickly decomposes to inorganic salts during subsequent growth in Li rich environments. The surface films formed in our simulations have a multilayer structure with regions rich in inorganic and organic salts located near the anode surface and the electrolyte interface, respectively, in agreement with depth profiling experiments. Our computed formation potentials 1.0 V vs. $Li/Li^+$ is also in excellent accord with experimental measurements. We have also calculated the elastic stiffness of the SEI films; we find that they are significantly stiffer than Li metal, but are somewhat more compliant compared to the graphite anode.



## 1. Introduction

As the global energy demand increases, developing energy storage systems with higher energy densities is becoming more and more critical. Rechargeable Li-ion batteries have been widely used in portable electronics due to their high gravimetric energy storage and now are being considered for critical applications such as heavy automotives and medical devices. Currently, the negative electrode material used in most Li-ion batteries is graphite, which forms lithium–graphite intercalation compounds (Li–GICs) [1,2]. During the first charge of the Li-ion battery, the electrolyte decomposes at the surface of the graphite anode. This forms a film composed of inorganic and organic electrolyte decomposition products, called the solid electrolyte interphase (SEI) [3]. While this layer imparts kinetic stability to the electrolyte against further reduction in successive cycles and thereby ensures good cyclability of the electrode, it leads to irreversible loss of Li and the capacity of the battery [4–8]. The composition, thickness, morphology, and compactness of the SEI all significantly affect battery performance [9,10]. The properties of the SEI become even more important during cycling at high rates and at deeper depth of discharge. In particular, during power cycling, large stresses build up in the electrode leading to cracking of the SEI films and graphite is again exposed to the electrolyte [11]. Growth of fresh SEI on the crack faces leads to further loss of capacity [8]. Therefore understanding the formation mechanisms, composition, structure and mechanical and transport properties of the SEI is critical for design of long-lived, high-performance batteries.

As discussed in detail in a recent review article on SEI, the picture of a real SEI inside a Li-ion battery has always been a blur [9,10]. Models proposed by Peled et al. [12], Aurbach et al. [13,14], and Edström et al. [15,16] suggest SEI to be a dense layer of inorganic components close to the anode, followed by a porous organic or polymeric layer close to the electrolyte phase. From an experimental point of view, since most of the characterization studies of the SEI are carried out *ex-situ*, it is difficult to know with a high degree of certainty whether the structure of the SEI is influenced by the artifacts of the measurement and processing techniques. Therefore detailed information of the composition and morphology of the SEI are currently under debate. For example, Leifer et al. very recently suggested an entirely new family of SEI products, which have not been identified in prior work using XPS and FT-IR [17]. Given the experimental difficulty in characterizing the SEI, a natural question to ask is whether computational models can be used to address issues related to the composition and structure of the SEI.

* Corresponding author. Tel.: +1 401 863 1475; fax: +1 401 863 9009.
*E-mail address:* Vivek_Shenoy@brown.edu (V.B. Shenoy).

0378-7753/$ – see front matter © 2011 Elsevier B.V. All rights reserved.
doi:10.1016/j.jpowsour.2011.05.061

Molecular simulations (MD) using chemically accurate methods can provide information on the reaction pathways, rates and byproducts of electrolyte decomposition reactions as well the composition and spatial distribution of the reduction products in the SEI films. However, most studies to date, that employ quantum simulations, have focused on modeling the former [18–20]. More recently *ab intio* MD studies have been used to study the early stages of SEI formation [21], but given the computational cost, these calculations cannot handle the sizes of typical SEI films (typically 10 nm or more). In this work, we employ a reactive force field potential, ReaxFF [22], to study the structure of the SEI formed when a Li metal anode is "dipped" in an electrolyte and in the case where Li atoms are introduced at the surface of the simulation box and allowed to interact with electrolyte molecules. In the ReaxFF that we employ in this work, atomic connectivity is determined by bond orders calculated from interatomic distances that are updated every MD step. This allows for bonds to break and form during the simulation. In order to account for non-bonded interactions such as van der Waals and Coulomb interactions for a system with changing connectivity, these interactions are calculated between every pair of atoms, irrespective of connectivity [23].

There are competing and parallel solvent reduction processes, which result in deposition of a number of organic and inorganic decomposition products on the surface of anode. To ensure that the reactive potential we have studied capture these fundamental processes, we first simulate several key reactions leading to primary and secondary decomposition products. We find that the reaction pathways and products we obtain are generally in agreement with first principles calculations and experiments. Having confirmed the ability of our approach to capture the "unit processes" leading to the formation of the SEI, we proceed to simulate the growth of the SEI when the electrolyte is exposed to Li anode or when Li atoms are introduced at a putative anode surface. Using these simulations we obtain the detailed structure of the SEI including its composition as a function of the distance from the anode surface. Experiments have shown that the SEI compositions and contents are a direct consequence of the electrolyte composition. We have therefore carried out these simulations with Ethylene Carbonate (EC), Dimethyl Carbonate (DMC) and mixtures of both. We find that lithium alkoxides appear in the SEI formed in DMC electrolytes, while $Li_2O$ and $Li_2CO_3$ appear in the SEI formed in EC (Fig. 5). Both solvents react to form several products, both $ROCO_2Li$ and ROLi species. Further reduction of $ROCO_2Li$ leads to the formation of surface $Li_2CO_3$. Consequently, the surface films formed in our simulations have a multilayer structure as confirmed by depth profiling and XPS [24], and are laterally non-uniform, as confirmed by in situ AFM [25]. Under the same conditions, the thickness of SEI formed with EC is more than DMC, indicating that the EC is more reactive, also in accord with observations [26,27]. Our simulations also allow us to compute the formation potential of the SEI for different electrolytes. Finally, a good SEI should be a compact layer adhering well to the anode. It should be elastic and flexible to accommodate non-uniform electrochemical behavior and active material breathing. At present, there is no information on the mechanical properties of the SEI and how these properties are related to the composition of the electrolyte. We have used our simulations to study the elastic properties of the SEI.

## 2. Simulation methods

MD simulations were performed using ReaxFF, which is a general bond-order-dependent potential that provides accurate descriptions of bond breaking and bond formation [22]. The main

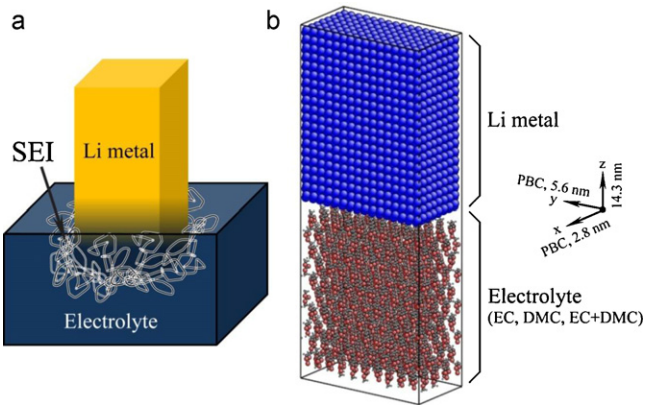


**Fig. 1.** (a) Schematic of a Li metal electrode dipped in an electrolyte. (b) Initial configuration of the cell used in our simulations.

difference between traditional nonreactive force fields and the one that we employ in this work is that the atomic connectivity is determined by bond orders calculated from interatomic distances that are updated every MD step. This allows for bonds to break and form during the simulation. In order to account for non-bonded interactions such as van der Waals and Coulomb interactions for a system with changing connectivity, these interactions are calculated between every pair of atoms, irrespective of connectivity, and any excessive close-range non-bonded interactions are avoided by the inclusion of a shielding term [23]. The force field used in the current work has been trained against the quantum-mechanical data for Li–C–O–H systems described in Han et al. [28] and was re-optimized recently. As we show below, this potential can provide the details of the variations of the composition of the SEI over nanometer length scales.

To model the formation of SEI, we have considered two types of simulations. In the first case, we model the fundamental electrolyte decomposition reactions that occur when Li metal is "dipped" in an electrolyte [12,29–31] as shown in Fig. 1(a). Here, as the Li atoms interact with the electrolyte, they transfer electrons to the electrolyte molecules forming organic and inorganic decomposition products. As we show below, the advantage of these simulations is that basic decomposition reactions can be studied without the need for "charging" the anode. The electrolyte at the equilibrium density of liquid phase is filled above single crystal bcc Li with dimensions ($8 \times 16 \times 20\ a_0^3$). The systems we consider are composed of 5120 Li atoms and about 800 electrolyte molecules. The size of the simulation box is approximately 3 nm × 6 nm × 14 nm. Periodic boundary conditions are enforced along the $x$ and $y$ directions (Fig. 1(b)). In the $z$ direction, a flat wall, which interacts with the atoms by generating a force in a direction perpendicular to the wall to prevent them from escaping during MD simulations, is introduced. In our simulations, charge transfer is performed by the charge equilibration (QEq) method [32] at every MD step. The temperature of the system is controlled by rescaling atomic velocities every 10 MD steps (each MD time step $\Delta t = 0.2$ fs). The system is heated up to the desired temperature during the first $5 \times 10^4$ MD steps (= 10 ps) and kept at constant temperature for 40 ps. Based on the bond information computed by the ReaxFF potential, a home-built program was developed to that identify the constituents of the SEI based on the number of bonds and charge state of each atom in a molecule.

In the second set of calculations, we simulate SEI formation during the charging process as $Li^+$ ions from the electrolyte combine with the electrons from the anode and the electrolyte molecules in the vicinity of the anode surface (typically less than a nanometer,

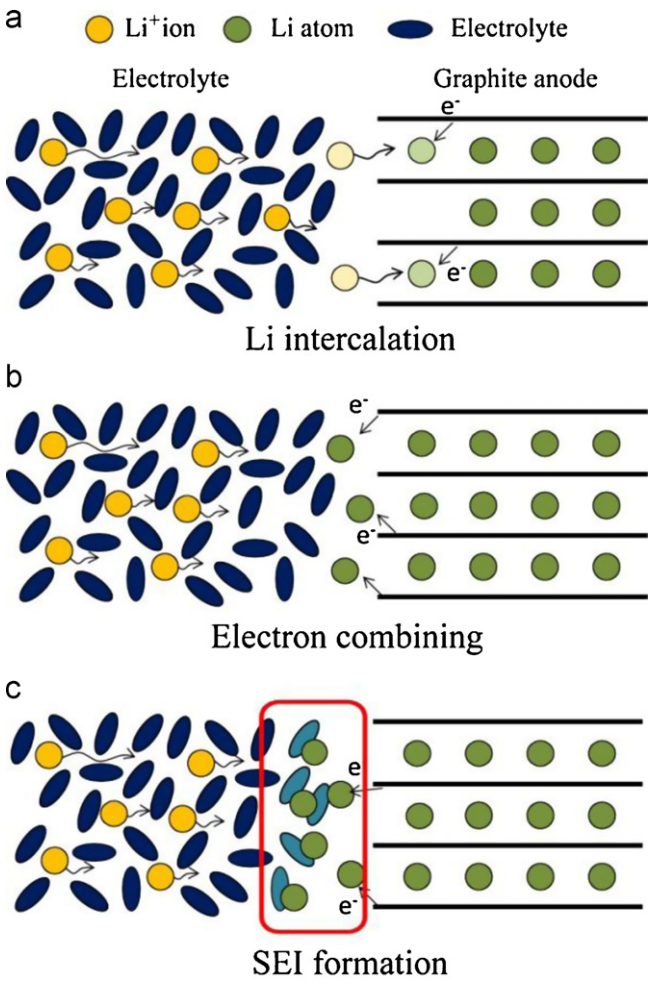


**Fig. 2.** Schematic depiction of the SEI formation during initial charging cycles.

which is the distance over which the electron can tunnel from the anode [33]). In our molecular simulations, it is difficult to confine the electrons to the anode and $Li^+$ ions to the electrolyte. However, since the electrons and $Li^+$ ions combine with the electrolyte to form the SEI only in the immediate vicinity of the anode, this difficulty can be circumvented by introducing Li atoms (or equivalently $Li^+ + e^-$) within a distance of 1 nm from the anode surface (Fig. 2). The atoms can combine with the electrolyte molecules to form the SEI products, thus mimicking the charging process. In our simulations, we introduce a certain number of Li atoms at the anode surface and allow them to react with electrolyte molecules. Li atoms are introduced every 1.0 ps at randomly selected locations on the bottom surface of the simulation cell ($x$–$y$ plane), whose size is 3.3 nm × 3.4 nm × 4.5 nm in $x$, $y$, and $z$ directions, and the temperature of the system is kept at 300 K by rescaling the temperature every 10 MD steps. This rate of introducing the Li atoms is sufficient to observe the initial stages of the SEI growth because the major reactions such as bond breaking and reformation between Li ions and electrolytes occur within a few ps [21]. As in the case of the first set of calculations, periodic boundary conditions are enforced in $x$ and $y$ directions. We note that the typical concentration or areal density of $Li^+$ ions at the surface of C anode is 3.63/nm$^2$ for zigzag edge or 6.28/nm$^2$ for armchair edge, which is significantly smaller that the concentration of Li atoms on the surface of Li metal (9.3/nm$^2$). As we discuss below, the concentration of Li atoms has a significant influence over the type of the SEI products that are formed.

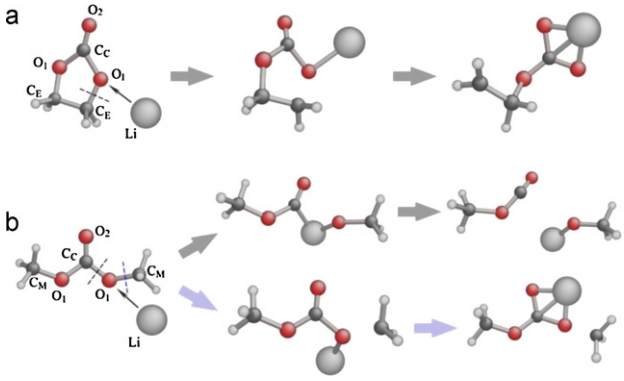


**Fig. 3.** Basic decomposition reactions for the case of (a) ethylene carbonate (EC), and (b) dimethyl carbonate (DMC) interacting with Li. The dashed lines indicate the bonds that are broken as a result of the reactions.

## 3. Results and discussion

### 3.1. Mechanisms for the formation of SEI components

The structure of the electrolyte molecules (EC and DMC) relaxed using the ReaxFF potential is in the first frame shown in Fig. 3. Comparing the computed structure with density functional theory (DFT) calculations and experiments (Table 1), we find that the potential captures all the bond lengths and angles very well. Next, we consider the key decomposition reactions that involve interaction of the electrolyte with Li atoms. To study these reactions, we introduce Li atoms randomly at distances >5 Å from the centroids of the electrolyte molecules and allow the molecules to interact at temperatures close to 500 K for 2 ps. We tried several sets of initial positions, but the results predominantly fall into the two categories shown in Fig. 3. As in the case of DFT calculations [21], the reactions occur in most cases within 1.0 ps or less. Fig. 3(a) shows the primary reaction pathways for a Li atom interacting with an EC molecule. The reaction results in the formation of a $LiOCO_2C_2H_4$ radical by means of breaking the $C_E$–$O_1$ bond, in agreement with previous DFT studies [18]. After the cleavage of this bond, the charge of the atoms, $C_E$ and $O_1$ changed from +0.016$e$ and −0.47$e$ to −0.23$e$ and −0.61$e$, respectively. As we discuss below, $LiOCO_2C_2H_4$ can further react to from molecules such as dilithium ethylene dicarbonate ($[LiOCO_2CH_2]_2$:LiEDC), lithium carbonate ($Li_2CO_3$) and $Li_2O$. Two primary pathways for the interaction of Li atoms with DMC are shown in Fig. 3(b). In one case, lithium methoxide ($LiOCH_3$) is formed as a result of the cleavage of the $C_C$–$O_1$ bond, while the other reaction leads to the formation of lithium methyl carbonate ($LiOCO_2CH_3$) as a result of the cleavage of the $C_M$–$O_1$ bond. The resulting molecule, $OCOCH_3$ is the precursor for the formation of CO and $LiOCH_3$ as discussed below. These results for the decomposition of DMC are in good agreement with the reaction suggested on the basis of experimental measurements [36,37].

Next we focus on secondary decomposition reactions that involve further interactions of the primary decomposition products in Fig. 3 with each other or with Li. The reaction pathway for the formation of LiEDC, Fig. 4(a), and a hydrocarbon gas molecule, $C_2H_4$ as a result of the interaction between two $LiOCO_2C_2H_4$ radicals is shown in Fig. 3(a). Generally, LiEDC is considered to be a primary component of the SEI in EC based electrolytes [38,39]. However, we find that this molecule can easily breakdown in the presence of Li atoms. As shown in Fig. 4(b), Li atoms directly attack the $O_1$–$C_E$ bond in LiEDC and dissociate it into lithium carbonate ($Li_2CO_3$) and $LiOCO_2C_2H_4$. The latter radical can further interact with Li atoms to eventually form two lithium carbonate molecules and an ethylene gas molecule. Lithium carbonate can further decompose (Fig. 4(c))

**Table 1**
Characteristics of ethylene carbonate (upper values) and dimethyl carbonate (lower values). The units of the length, charge and angle are Å, $e$ and°, respectively.

| | This work | Brown [34] | Wang et al. [18] | Tasaki et al. [19] | Xing et al. [35] |
|---|---|---|---|---|---|
| $O_2{=}C_C$ | 1.152 | 1.15 | 1.187 | – | 1.19 |
| | 1.159 | – | – | – | 1.21 |
| $O_1{-}C_C$ | 1.495 | 1.33 | 1.353 | – | 1.36 |
| | 1.460 | – | – | – | 1.34 |
| $O_1{-}C_E$ | 1.506 | 1.40 | 1.426 | – | 1.44 |
| $O_1{-}C_M$ | 1.458 | – | – | – | 1.44 |
| $qO_1$ | −0.469 | – | – | −0.36 | −0.55 |
| | −0.489 | – | – | −0.39 | – |
| $qO_2$ | −0.533 | – | – | −0.50 | −0.56 |
| | −0.616 | – | – | −0.55 | – |
| $qC_C$ | 0.955 | – | – | 0.80 | 1.01 |
| | 0.961 | – | – | 0.92 | – |
| $qC_E$ | 0.016 | – | – | 0.01 | −0.05 |
| $qC_M$ | −0.061 | – | – | −0.15 | – |
| $\angle O_1C_CO_2$ | 135.7 | 124.1 | 124.7 | – | – |
| | 131.6 | – | – | – | – |
| $\angle C_CO_1C_E$ | 125.6 | 109 | 110.7 | – | – |
| $\angle C_CO_1C_M$ | 127.4 | – | – | – | – |

in the presence of Li atoms to form $Li_2O$ and a CO molecule. Presence of CO has been detected in recent experimental studies [40]. Fig. 4(d) shows the mechanism for the formation of CO and a $LiOCH_3$ molecule from the $OCOCH_3$ radical, which is one of the primary structures that results from the reaction between a DMC and a Li (Fig. 3(b)). Finally, Fig. 4(e) shows the formation mechanism of a $Li_2CO_3$ molecule from the $LiOCO_2CH_3$ radical. Having verified that our MD simulations predict primary and secondary decomposition reactions in agreement with available DFT calculations [18] and pathways deduced from experiments [36], we now proceed to study the structure of the SEI when all of these reactions can simultaneously occur. Note that given the computational cost, quantum mechanical approaches cannot be used to determine the structure of the ∼10 nm thick SEI films, but as we show next, the molecular simulations we employ can predict the spatial variations in the composition of the constituents of SEI, their formation potentials and elastic properties.

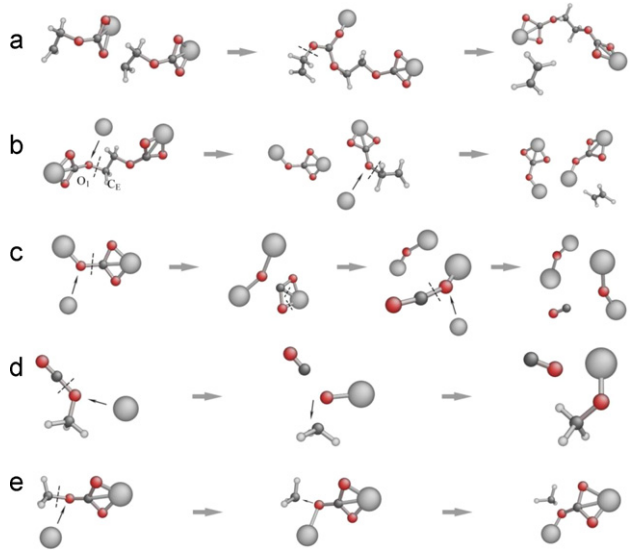


**Fig. 4.** Secondary decomposition reactions for the key SEI components. (a) Formation of LiEDC and a $C_2H_4$ molecule from two $LiOCO_2C_2H_4$ radicals. (b) Two $Li_2CO_3$ and a $C_2H_4$ formed from a LiEDC molecule interacting with additional Li atoms. (c) Two $Li_2O$ and a CO molecule formed from $Li_2CO_3$. (d) A $LiOCH_3$ and a CO molecule formed from $OCOCH_3$. The dashed lines are the bonds that are broken as a result of the reactions. Dark gray, white, red and big light gray atoms denote C, H, O and Li, respectively.

### 3.2. Effects of electrolytes on the evolution of the SEI

The atomic configurations after 40 ps NVT-MD simulation at 300 K and 500 K for the electrolyte–Li metal system are shown in Fig. 5. The constituent atoms are color-coded according to their charge, which allows us to readily distinguish the SEI region from the electrode; Li atoms are neutral in the electrode and are in a positive charge state (>+0.1$e$) once they interact with the electrolyte and become part of the SEI. Our simulations (Fig. 5(b)) show that the SEI films grow faster in the case of EC compared to DMC, with EC + DMC mixtures falling in between. As shown in Fig. 5(c), the density of Li consumed in the SEI tends to an asymptotic limit, which depends on the type of electrolyte but weakly on the temperature. The saturation values lie between 0.1 and 0.13 g/cm$^3$, which is much lower than the density of Li metal (0.53 g/cm$^3$). The density of Li incorporated in the case of EC is more than that amount consumed in DMC and the case of EC + DMC mixtures lies in between. This result agrees with the experimental observations that show that EC is more reactive compared to DMC [26,27].

In the case of Li metal, the constituents of the SEI components are highly dependent on the type of the electrolyte as shown in Fig. 6. The SEI in the case of EC is composed largely of $Li_2O$ and $Li_2CO_3$ along with trapped gas molecules, $C_2H_4$ and CO. We find that while LiEDC is formed in the very early stages of SEI growth, it decomposes into other byproducts by interacting with Li atoms of the metal anode. Since LiEDC is considered to be a major component of SEI in graphite anodes, we hypothesize that it would not decompose in the Li-poor environment found at the surface of graphite compared to the case of Li anode. To test this hypothesis, we carried out SEI growth simulations using the approach sketched in Fig. 2, where Li atoms are introduced at the putative anode surface. Indeed, as shown in Fig. 7 we find copious formation of LiEDC and $Li_2CO_3$ at early stages of SEI growth. As the growth of the SEI progresses, the quantity of $Li_2CO_3$ keeps increasing, but the number of the LiEDC in this case peaks around 5.0 atoms/nm$^2$ and subsequently saturates. The amount of $Li_2O$ in the SEI increases at the expense of LiEDC. In the case of Li metal anode, given the high concentration of Li atoms, almost all of the LiEDC that is formed is instantaneously consumed. Taken together, the results in Figs. 6 and 7 show that Li concentration plays an important role in determining the composition of SEI in the case of EC. For the case of high Li concentration as in Li metal, the bond between carbonate ($CO_3$) and ethylene ($C_2H_4$) can easily be broken by Li atoms leading to formation of hydrocarbon gases. The carbonate group that is left behind, reacts with additional Li ions and consequently dissociates into the different types of Li salt such as $Li_2CO_3$ and $Li_2O$ as shown in Fig. 4(c). Very recent exper-

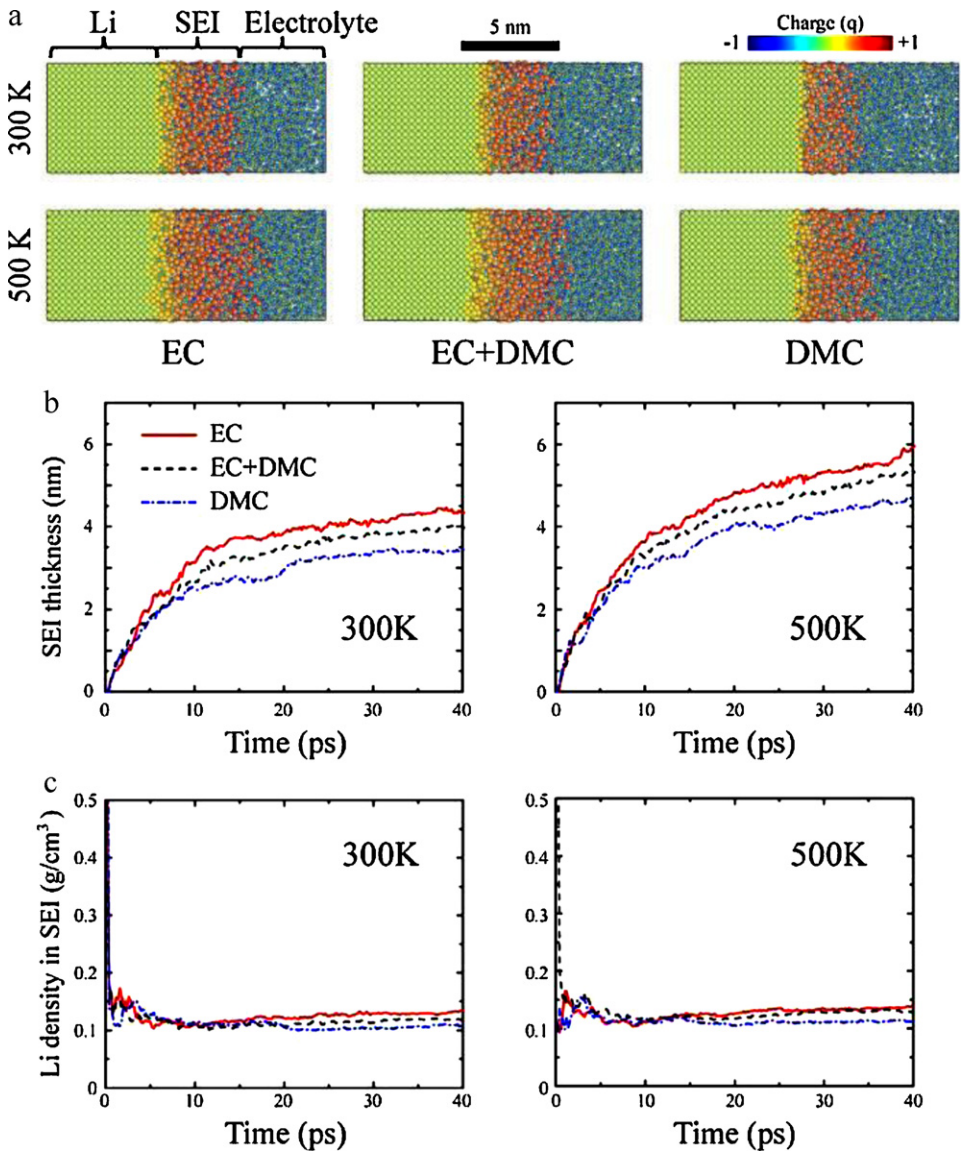


**Fig. 5.** (a) Atomic configuration, (b) evolution of the thickness of the SEI and (c) Li density in the SEI formed between Li metal and electrolytes (EC, EC + DMC, and DMC) at different temperatures (300 K and 500 K). Snapshots in (a) are obtained after 40 ps of NVT MD simulations. The atoms are color-coded according to their charge state (green is neutral).

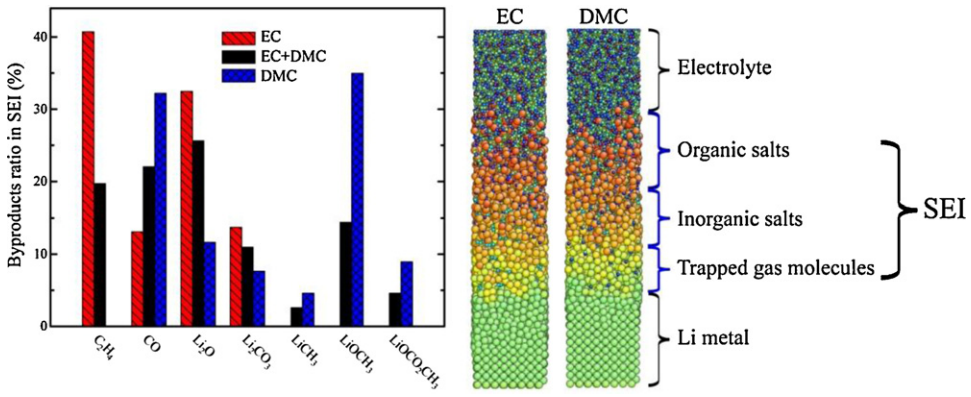


**Fig. 6.** Distribution of the SEI components for different electrolytes (left). Atomic configurations from MD simulations; the components of the SEI are identified (right).

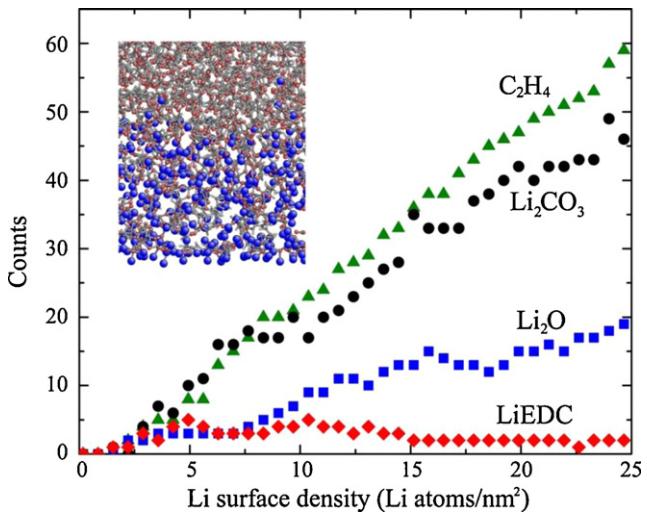


**Fig. 7.** The evolutions of EC based SEI components with increasing Li density. Inset is a snapshot of the atomic configurations when the Li (blue atoms) surface density is 20/nm$^2$.

imental work on the composition of SEI [41] on electrodeposited Li metal indeed shows that $Li_2CO_3$ and $Li_2O$ are the primary components of the SEI in agreement with our calculations. While this work found the presence of LiOH and $Li_3N$ in SEI films (due to exposure to air), LiEDC was not detected in the SEI films confirming the predictions of our work.

The SEI in the case of DMC is composed of $Li_2O$, $LiOCO_2CH_3$, $Li_2CO_3$, and $LiCH_3$, with $LiOCH_3$ being the dominant constituent [38,39]. If the dissociation follows the first of the reaction pathways shown in Fig. 3(b), two $LiOCH_3$ molecules can be formed along with a CO molecule. However, if a Li atom reacts with the carbonate part of the DMC molecule (which corresponds to the cleavage of the $C_M$–$O_1$ bond as shown in Fig. 3(b)), the types of the byproducts that are formed are determined by the number of Li atoms that replace the methyl radicals. $Li_2CO_3$ is created when two Li atoms replace two methyl radicals (Fig. 4(e)), while $LiOCO_2CH_3$ is formed when only methyl radical is replaced (Fig. 4(d)). As in the case of EC, where $C_2H_4$ molecules are formed during decomposition, we can expect the formation of ethane ($C_2H_6$) from DMC, but we did not detect it to any significant extent. This is because of the small probability for the completion of the reaction between the two methyl radicals, $\bullet CH_3 + \bullet CH_3 \rightarrow C_2H_6$, which is needed for the formation of ethane. Instead, $LiCH_3$ is formed when Li atoms combine with the methyl radical [42]. In DMC, CO turns out to be the major gas molecule produced (which constitutes 31.6% of the total amount of the SEI components), in good agreement with the previous experimental work [43]. When Li reacts with the mixture electrolyte of EC and DMC, the type of SEI components follow the order $Li_2O > LiOCH_3 > Li_2CO_3 > LiOCO_2CH_3 > LiCH_3$. The reason why $Li_2O$ is the most abundant component is because the secondary reactions of Li atoms with both EC and DMC decomposition products lead to the formation of $Li_2O$ molecules.

Next, we consider the spatial distribution of the SEI components in Fig. 8. The surface films formed in our simulations have a multilayer structure in agreement with depth profiling experiments. We find that the gases formed as a result of electrolyte decomposition reactions are trapped near the Li metal side. Given the short time scale of our simulations, these gases are not able to diffuse through the SEI; in real-life, these molecules can escape from the SEI-electrode interface by diffusion. Inorganic Li salts such as $Li_2CO_3$ and $Li_2O$ tend to be closer to the Li metal electrode, while organic Li

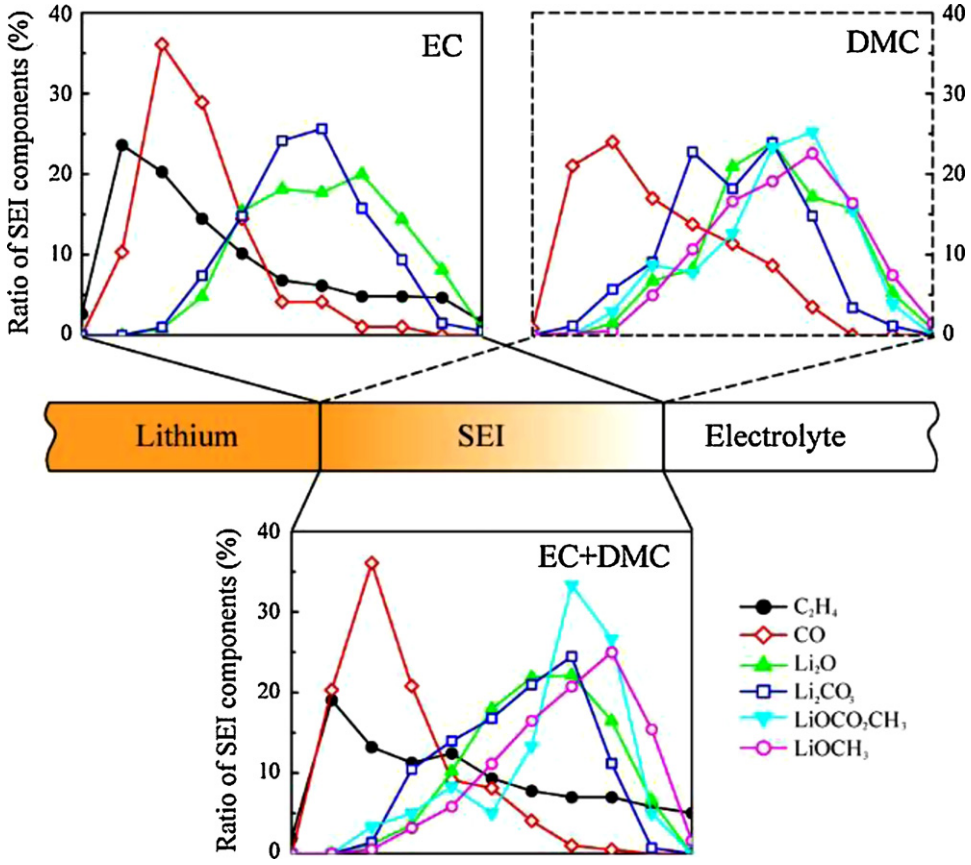


**Fig. 8.** Spatial distribution of the SEI components for different electrolytes.

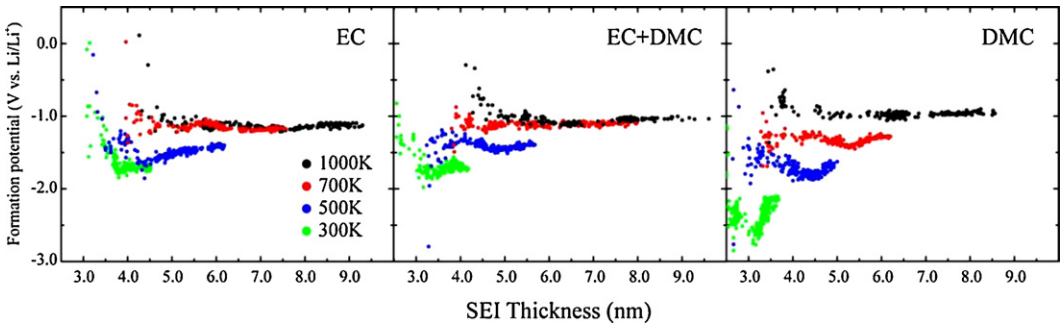


**Fig. 9.** The formation potential for different electrolytes plotted as a function of the thickness of SEI films.

salts such as $LiOCH_3$ and $LiOCO_2CH_3$ are found at the SEI-electrolyte interface in agreement with experiments [12]. The reason why inorganic salts with high Li content compared to organic salts are found near the electrode is that these salts and hydrocarbon gases result from the decomposition of the primary SEI products as they combine with additional Li atoms. High Li content at the surface of the anode allows these reactions to proceed at the higher rate compared to the electrolyte–SEI interface, which is dominant in primary decomposition products.

### 3.3. Effects of electrolytes on the SEI properties

Our simulations show that Li reacts spontaneously with the electrolyte to produce decomposition products which are more thermodynamically stable. The difference in the energy of the reactants and the products gives the so-called "SEI formation potential". In order to quantify the formation potential, we use the potential energy computed as a function of the SEI thickness in the equation $E_f(d) = \frac{E(d)-(E_{Li}+E_{electrolyte})}{N_{Li^+}(d)}$, where $N_{Li+}$ is the number of $Li^+$ ions that have reacted to form the SEI and $E(d)$ is the potential energy of the SEI as a function of its thickness $d$, $E_{Li}$ denotes the energy of Li atom in metal and $E_{electrolyte}$ is the potential energy of the electrolyte prior to decomposition.

For the electrolyte–Li-metal system, Fig. 9 shows the SEI formation potential, $E_f$, as a function of the SEI thickness $d$ for EC, DMC and EC + DMC for different temperatures. In all cases, the formation potential tends to an asymptotic limit, which depends weakly on temperature. The saturation values lie around 1.0 V vs. $Li/Li^+$, in good agreement with the experimental measurements that are generally in the range 0.8–1.0 V vs. $Li/Li^+$ [44–47]. The potential for DMC, EC and EC + DMC are 0.9 V vs. $Li/Li^+$, 1.1 V vs. $Li/Li^+$ and 1.0 V vs. $Li/Li^+$, respectively.

A good SEI should be elastic and flexible to accommodate non-uniform electrochemical behavior and active material breathing. To estimate the mechanical compliance of the SEI, we now turn to the calculation of the elastic constants of the SEI. To achieve this task, we first extract the SEI region from the simulation box excluding both Li metal and electrolyte region as shown schematically in Fig. 10. The extracted sample is then equilibrated using NPT molecular dynamics at 300 K and 1 atm for 40 ps. The elastic constants ($C_{ij}$) are obtained by calculating the change in stress as small strains ranging from 0.1 to 1.0% are applied to the sample along the coordinate axes. From the knowledge of the elastic constants ($C_{ij}$), bulk modulus ($B$) and shear modulus ($G$) are then calculated using the equation

$$B = \frac{C_{11} + C_{22} + C_{33} + 2(C_{12} + C_{13} + C_{23})}{9}$$

$$G = \frac{C_{11} + C_{22} + C_{33} - C_{12} - C_{13} - C_{23}}{15} + \frac{C_{44} + C_{55} + C_{66}}{5}$$

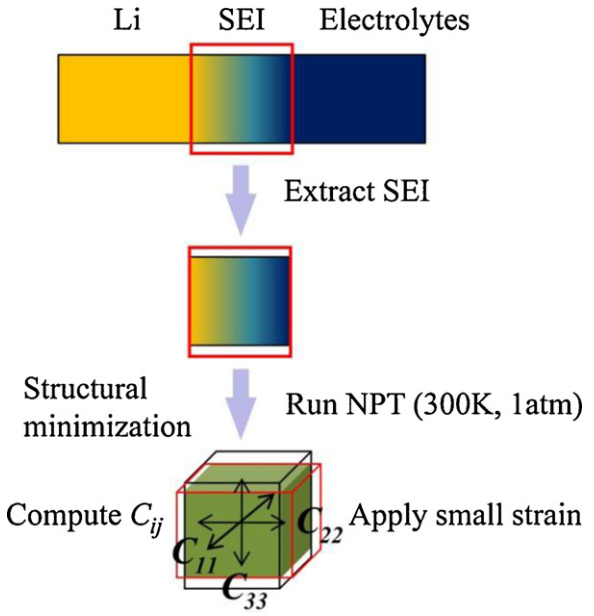


**Fig. 10.** The schematic of the method used for computing the elastic properties of the SEI.

**Table 2**
Mechanical properties of SEI films.

| | $SEI_{EC}$ | $SEI_{EC+DMC}$ | $SEI_{DMC}$ | Li metal | Graphite [48] |
|---|---|---|---|---|---|
| $E$ (GPa) | 18.54 | 15.99 | 14.96 | 4.9 | 32.47 |
| $B$ (GPa) | 14.64 | 10.24 | 11.47 | 11 | 29.29 |

The Young's modulus is then computed by assuming isotropic linear elastic stress–strain relations. Table 2 shows the elastic properties computed in the three cases. According to our results, the Young's modulus is somewhat larger for the SEI formed in the case of EC compared to the case of DMC. Note also that the SEI films are more compliant to typical anode materials (graphite $E$ = 32.47 GPa), but is significantly stiffer than Li. The elastic properties we have computed here can be used in continuum models for stress generation in Li-ion battery anodes.

## 4. Summary and conclusions

In summary, we have used molecular dynamics simulations using the ReaxFF potential to simulate the formation of SEI on Li metal anodes and by introducing Li atoms randomly at the surface of our simulation cell. The latter set of simulations is used to assess the role of Li density on the formation of SEI films. While quantum simulations can accurately predict the kinetics of individual reactions, they cannot be used to study competing reactions leading

to the formation of complex SEI films typically several nanometers thick. In our MD simulations, we first considered the primary and secondary decomposition reactions that involve Li and the electrolyte molecules and showed that our potential correctly captures the reaction pathways and byproducts. We then simulated the formation of SEI allowing electrolytes composed of EC, DMC and EC + DMC with Li atoms from at the anode surface. Using our simulations, we studied the distribution of organic and inorganic salts as a function of the distance from the anode surface. We find that $Li_2CO_3$ and $Li_2O$ are the primary components of the SEI in Li metal anodes when EC is used as an electrolyte. LiEDC that is formed in the early stages of SEI formation decomposed into inorganic salts and hydrocarbon molecules in a Li rich environment. In the case of DMC, we find $LiOCH_3$ to be the dominant component of the SEI, in excellent agreement with experiments [37]. Our simulations show that inorganic salts are found closer to the anode surface while the region near the electrolyte–SEI interface is rich in organic salts. Using our simulations we find the SEI formation potential to be in the range 0.9–1.0 V vs. $Li/Li^+$, also in accord with experiments. Finally, we have computed the elastic properties of the SEI; SEI is found to be significantly stiffer than Li metal, but is somewhat softer than the graphite anode. Cracking of SEI during power cycling is one of the causes for the loss of capacity of Li-ion batteries. Work is currently underway to include the properties computed here in continuum models for progressive crack propagation in electrode particles during charge and discharge. Finally, while Li salts are known to play an important role in the formation of SEI, we have only studied the decomposition of the bare electrolyte. Development of new reactive potentials for P and F will allow one to extend the present work to account for the presence of salts.

## Acknowledgements

We gratefully acknowledge support from the NSF. Computational support for this research was provided by the grant TG-DMR090098 from the TeraGrid advanced support program.

## References

[1] R.A. Huggins, Advanced Batteries-Materials Science Aspects, Springer, 2009.
[2] J.R. Dahn, Phys. Rev. B 44 (1991) 9170–9177.
[3] E. Peled, J. Electrochem. Soc. 126 (1979) 2047–2051.
[4] R. Kostecki, F. McLarnon, J. Power Sources 119–121 (2003) 550–554.
[5] L.J. Hardwick, M. Marcinek, L. Beer, J.B. Kerr, R. Kostecki, J. Electrochem. Soc. 155 (2008) A442–A447.
[6] E. Markervich, G. Salitra, M.D. Levi, D. Aurbach, J. Power Sources 146 (2005) 146–150.
[7] D. Aurbach, B. Markovsky, I. Weissman, E. Levi, Y. Ein-Eli, Electrochim. Acta 45 (1999) 67–86.
[8] J. Vetter, P. Novák, M.R. Wagner, C. Veit, K.-C. Möller, J.O. Besenhard, M. Winter, M. Wohlfahrt-Mehrens, C. Vogler, A. Hammoushe, J. Power Sources 147 (2005) 269–281.
[9] P.B. Balbuena, Y. Wang, Lithium-Ion Batteries: Solid–Electrolyte Interphase, Imperial College Press, London, 2004.
[10] P. Verma, P. Maire, P. Novák, Electrochim. Acta 55 (2010) 6332–6341.
[11] R. Grantab, V.B. Shenoy, J. Electrochem. Soc, doi:10.1149/1.3601878 (2011).
[12] E. Peled, D. Golodnitsky, G. Ardel, J. Electrochem. Soc. 144 (1997) L208–L210.
[13] D. Aurbach, J. Power Sources 89 (2000) 206–218.
[14] A. Zaban, D. Aurbach, J. Power Sources 54 (1995) 289–295.
[15] E. Edström, M. Herstedt, D.P. Abraham, J. Power Sources 153 (2006) 380–384.
[16] A.M. Andersson, A. Henningson, H. Siegbahn, U. Jansson, K. Edström, J. Power Sources 119–121 (2003) 522–527.
[17] N. Leifer, M.C. Smart, G.K.S. Prakash, L. Gonzalez, L. Sanchez, K.A. Smith, P. Bhalla, C.P. Grey, S.G. Greenbaum, J. Electrochem. Soc. 158 (2011) A471–A480.
[18] Y. Wang, S. Nakamura, M. Ue, P.B. Balbuena, J. Am. Chem. Soc. 123 (2001) 11708–11718.
[19] K. Tasaki, S.J. Harris, J. Phys. Chem. C 114 (2010) 8076–8083.
[20] O. Borodin, G.D. Smith, J. Phys. Chem. B 110 (2006) 22773–22779.
[21] K. Leung, J.L. Budzien, Phys. Chem. Chem. Phys. 12 (2010) 6583–6586.
[22] A.C.T. van Duin, S. Dasgupta, F. Lorant, W.A. Goddard III, J. Phys. Chem. A 105 (2001) 9396–9409.
[23] K. Chenoweth, A.C.T. van Duin, W.A. Goddard III, J. Phys. Chem. A 112 (2008) 1040–1053.
[24] K. Kanamura, H. Tamura, S. Shiraishi, Z. Takehara, J. Electroanal. Chem. 394 (1995) 49–62.
[25] D. Aurbach, Y. Cohen, J. Phys. Chem. B 104 (2000) 12282–12291.
[26] Y. Ein-Eli, B. Markovsky, D. Aurbach, Y. Carmeli, H. Yamin, S. Luski, Electrochim. Acta 39 (1994) 2559–2569.
[27] K. Tasaki, J. Phys. Chem. B 10 (2005) 2920–2933.
[28] S.S. Han, A.C.T. van Duin, W.A. Goddard III, H.M. Lee, J. Phys. Chem. A 109 (2005) 4575–4582, A.C.T. van Duin et al., to be published.
[29] K. Nishikawa, T. Mori, T. Nishida, Y. Fukunaka, M. Rosso, T. Homma, J. Electrochem. Soc. 157 (2010) A1212–A1217.
[30] D. Aurbach, B. Markovsky, M.D. Levi, E. Levi, A. Schechter, M. Moshkovich, Y. Cohen, J. Power Sources 81–82 (1999) 95–111.
[31] Y.S. Cohen, Y. Cohen, D. Aurbach, J. Phys. Chem. B 104 (2000) 12282–12291.
[32] A.K. Rappe, W.A. Goddard III, J. Phys. Chem. 95 (1991) 3358–3363.
[33] C. He, W. Wang, S. Deng, N. Xu, Z. Li, G. Chen, J. Peng, J. Phys. Chem. A 113 (2009) 7048–7053.
[34] C.J. Brown, Acta Crystallogr. 7 (1954) 92–96.
[35] L. Xing, W. Li, C. Wang, F. Gu, M. Xu, C. Tan, J. Yi, J. Phys. Chem. B 113 (2009) 16596–16602.
[36] D. Aurbach, E. Zingigrad, Y. Cohen, H. Teller, Solid State Ionics 148 (2002) 405–416.
[37] G.V. Zhuang, H. Yang, P.N. Ross Jr., K. Xu, T.R. Jow, Electrochem. Solid State Lett. 9 (2006) A64–A68.
[38] D. Aurbach, M.D. Levi, E. Levi, A. Schechter, J. Phys. Chem. B 101 (1997) 2195–2206.
[39] G.V. Zhuang, K. Xu, H. Yang, T.R. Jow, P.N. Ross Jr., J. Phys. Chem. B 109 (2005) 17567–17573.
[40] M. Onuki, S. Kinoshita, Y. Sakata, M. Yanagidate, Y. Otake, M. Ue, M. Deguchi, J. Elecrochem. Soc. 155 (2008) A794–A797.
[41] T. Momma, H. Nara, S. Yamagami, C. Tatsumi, T. Osaka, J. Power Sources 196 (2011) 6483–6487.
[42] H. Gérard, A. de la Lande, J. Maddaluno, O. Parisel, M.E. Tuckerman, J. Phys. Chem. A 110 (2006) 4787–4794.
[43] H. Yoshida, T. Fukunaga, T. Hazama, M. Terasaki, M. Mizutani, M. Yamachi, J. Power Sources 68 (1997) 311–315.
[44] J.S. Gnanaraj, R.W. Thompson, S.N. Iaconatti, J.F. DiCarlo, K.M. Abraham, Electrochem. Solid-State Lett. 8 (2005) A128–A132.
[45] M. Inabu, Z. Siroma, Y. Kawatate, A. Funabiki, Z. Ogumi, J. Power Sources 68 (1997) 221–226.
[46] J.O. Besenhard, M. Winter, J. Yang, W. Biberacher, J. Power Sources 54 (1995) 228–231.
[47] H. Bryngelsson, M. Stjerndahl, T. Gustafsson, K. Edström, J. Power Sources 174 (2007) 970–975.
[48] Y. Qi, H. Guo, L.G. Hector Jr., A. Timmons, J. Electrochem. Soc. 157 (2010) A558–A566.